ZnO particles of wurtzite structure as a component in ZnO/carbon nanotube composite

2009 J. Phys.: Condens. Matter 21 445801

(http://iopscience.iop.org/0953-8984/21/44/445801)

J. Phys.: Condens. Matter **21** (2009) 445801 (10pp) doi:10.1088/0953-8984/21/44/445801

ZnO particles of wurtzite structure as a component in ZnO/carbon nanotube composite

M Baibarac[1], I Baltog[1], T Velula[1], I Pasuk[1], S Lefrant[2] and N Gautier[2]

[1] National Institute of Materials Physics, Laboratory of Optics and Spectroscopy, PO Box MG-7, RO-77125 Bucharest, Romania
[2] Institut des Matériaux Jean Rouxell, 2 rue de la Houssinière, BP 32229, F-44322 Nantes, France

Received 22 July 2009, in final form 21 September 2009
Published 15 October 2009
Online at stacks.iop.org/JPhysCM/21/445801

Abstract
Composites based on carbon nanotubes and ZnO particles with needle shapes were prepared for applications in energy storage. Depending on the temperature (85 or 25 °C) at which the reaction between NaOH and $ZnCl_2$ was carried out, particles with two different morphologies: needle-shaped (NS) and double-pyramid-shaped (DPS), respectively, are obtained. Scanning electron microscopy, photoluminescence, UV–Vis absorption spectroscopy, x-ray diffraction and Raman light scattering studies reveal that the NS and DPS particles belong to ZnO with wurtzite (WZ) structure and ε-$Zn(OH)_2$ as precursors of ZnO, respectively. Using the ZnO/carbon nanotube composite as a negative electrode and an electrolytic solution containing $LiPF_6$, the charge–discharge characteristics of rechargeable lithium ions cells were determined. Additional information concerning the electrochemical reactions at the interface of the two electrodes was obtained by cyclic voltammetry.

(Some figures in this article are in colour only in the electronic version)

1. Introduction

In the last ten years, a great deal of effort has been devoted to the preparation and characterization of ZnO nanoparticles and their use as active components in different composites [1, 2]. ZnO, with a wide bandgap (3.37 eV) in bulk, is an attractive semiconductor material for nano-electronic and photonic applications [3, 4]. A large variety of ZnO nanostructured morphologies (nanowires, nanorods, tetrapods, nanoribbons/belts, nanorings, nanohelixes, nanosheets, hierarchical nanostructures, nanoellipsoids, nanotubes, etc) have been reported. According to the reaction environment, the particles produced may have a variety of crystal habits mainly determined by the ratio of the growth rates of each facet. Anisotropic growth dictates the crystallographic structure of the solid material and, as controlled by the nucleation process, is restricted to the nanometer size scale. Despite the vast literature dedicated to the growth of ZnO particles of different shapes and sizes, prediction of the final architecture is still problematic. As a general rule, using a suitable surfactant, surfactant mixture or capping molecules that selectively adsorb onto specific planes of growing particles, induces symmetry-breaking steps that lead to particles of different sizes and shapes.

Three crystalline structures, hexagonal wurtzite (WZ), cubic zinc blende (ZB) and cubic rock salt (RS), are reported for ZnO [1–3]. As a bulk crystal, ZnO grows in the WZ phase only, which undergoes a transition to the RS phase under a hydrostatic pressure of about 9 GPa [4–7]. WZ and ZB are quite similar phases. They have the same local tetrahedral atomic layout and start to differ only in their third-nearest-neighbor atomic arrangement. Due to this, the total energy difference between the WZ and ZB phases is usually very small (approx. a few meV/atom). The ZB structure has a lower ionicity compared to the WZ structure.

ZnO may be used in diverse applications alone or as a component of different composites. The combination of ZnO with carbon-based materials is of great interest. Beginning with 2005, one intensely developed topic was that of the preparation of composites based on carbon

nanotubes (CNs) and ZnO [8–13]. Two mechanisms have been proposed for the attachment of ZnO nanoparticles to CNs: non-covalent functionalization [9] and electrostatic coordination [10]. The main methods used for assembling ZnO onto the surface of carbon nanotubes are based on pulsed-laser deposition [14], chemical vapor deposition [15], microwave irradiation heating [16], a mechanical–chemical route [13], electrochemical way [17] and wet chemistry [18]. In this framework, wet chemistry proved to be an attractive method—it allows the synthesis of both ZnO particles of different shapes and sizes and ZnO/CN composites with low cost and without specific equipment. A review of the relevant literature indicates that, until now, composites based on CNs and ZnO nanoparticles with wires, rods, belts and flower-like shapes have been synthesized [19, 20]. Such syntheses need subtle manipulation of the parameters of the chemical reaction leading to ZnO particles of different sizes and shapes. An efficient combination with CNs requires these to be well dispersed in the chemical mixture used for ZnO generation and the unbinding of the nanotube bundles in isolated tubes needs a surfactant as dispersing agent. In this context the question arises: how does the wet chemical synthesis of ZnO particles proceed in the presence of CNs when the added surfactant can be both adsorbed selectively on specific crystalline planes of growing particles and interacts with the nanotubes during the dispersion process? In this framework, we report new data concerning the preparation of composites based on different types of CNs (single-walled carbon nanotubes (SWNTs), double-wall carbon nanotubes (DWNTs) and multi-wall carbon nanotubes (MWNTs)) and ZnO particles. The prepared composites were characterized by scanning electron microscopy (SEM), Raman light scattering, photoluminescence, x-ray diffraction and UV–vis absorption spectroscopy. The work reveals that the presence of CNs in the synthesis chemical mixture changes the growth mechanism that has, as a result, the formation of particles in two morphological forms: double-pyramid-shaped (DPS) associated with ε-$Zn(OH)_2$ as the precursor of ZnO and needle-shaped (NS) which are ZnO particles with wurtzite structure (WZ). The composite ZnO/CNs, once obtained, is used as the active material in rechargeable lithium ion batteries whose performance is tested by charge–discharge cycles.

2. Experimental details

All chemical compounds used in this paper, namely zinc chloride ($ZnCl_2$), sodium hydroxide (NaOH), sodium dodecyl sulfate (SDS), single-walled carbon nanotubes (SWNTs), double-wall carbon nanotubes (DWNTs) and multi-wall carbon nanotubes (MWNTs), were of Aldrich provenance. ZnO particles of micronic mean size and different shapes were obtained using the growing procedure described in [21] with some modifications consisting of: (i) the presence of SDS as the third reagent; (ii) the performance of the synthesis at 25 and 85 °C and (iii) the presence of CNs (SWNTs, DWNTs, MWNTs) as the fourth reactant.

For a ZnO sample prepared in the presence of SDS, the procedure involved several stages: (i) an aqueous solution of [NaOH (4 M; 30 ml) +SDS (0.2 M; 5 ml)] was added drop by drop to an aqueous solution of $ZnCl_2$ (1 M; 20 ml) under vigorous stirring for 15 min at 3 °C; (ii) this mixture, diluted with water to 100 ml and brought to room temperature, becomes whitish under mild continuous stirring for 1.5 h; (iii) the mixture, which on formation of the ZnO particles becomes whitish, was left standing for 5 h at 85 or 25 °C and (iv) subsequently a white product, containing ZnO particles, was collected on a filter paper, washed with deionized water and dried in vacuum at ambient temperature. The resulting product was labeled sample 1 (S_1) if the third stage was carried out at 85 °C or sample 2 (S_2) if the third stage was done at 25 °C. The procedure is similar when SDS and CNs are used as additional reagents of synthesis For the preparation of the ZnO/CNs composites, 20 mg of CNs (SWNTs, DWNTs and MWNTs) were added to the SDS solution which then were ultrasonicated for 30 min. All these steps were carried out in order to obtain a soluble sample of the type SDS non-covalent functionalized CNs, which permits a better interaction with the synthesis mixture. Thus, we have obtained ZnO/CNs samples labeled 3 (S_3) and 4 (S_4) when the crystallization temperatures were 85 and 25 °C, respectively. The novelty is that the powders (S_1; S_3) and (S_2; S_4) contain particles of different sizes and shapes, needle-shaped (NS) and double-pyramid-shaped (DPS), respectively.

The products obtained were analyzed by Raman spectroscopy at room temperature in backscattering geometry under excitation light of 676 and 1064 nm. For the former excitation wavelengths, a Jobin Yvon T64000 Raman spectrophotometer was used. It was equipped with a microprobe allowing the laser spot to be focused on the sample within a micrometer scale. For the 1064 nm excitation wavelength an FT Raman Bruker RFS 100 spectrophotometer was used. This allowed us to investigate a sample area of 1 mm^2. PL spectra at room temperature (RT) and liquid nitrogen temperature (LNT) spectra were recorded under excitation light of 330 nm in right angle geometry using a Horiba Jobin Yvon Fluorolog-2 spectrometer, model FL 3-22. UV–vis absorption spectra were obtained with a Perkin Elmer spectrophotometer, Lambda 90 model. SEM investigations were carried out using microscopes of the type Philips SEM 505. The phase structures of the as-synthesized products were examined by the use of a x-ray diffractometer (XRD) D8 Advanced model from Bruker.

Cyclic voltammetry and charge/discharge tests were carried out using a potentiostat/galvanostat model VOLTALAB 80 from Radiometer Analytical. To fabricate the negative electrode (anode), we used ZnO nanoparticles or the ZnO/SWNTs composites (80%, as active material), poly(vinylidene fluoride) (5 wt%, as binder), super-P carbon (15 wt%), dibutyl phthalate (DBP, two drops) and 1 ml acetone, which were mixed and stirred for 24 h to yield a homogeneous paste. The paste was tape-cast onto a glass surface and the acetone allowed to evaporate. The resulting film was peeled off and washed with diethyl ether to remove the DBP. Lithium foil (0.38 mm thickness; area 2.03 cm^2) was used as the positive electrode (cathode). The electrolyte used was a 1 M solution of $LiPF_6$ in a 50:50 mixture in volume of ethylene carbonate and

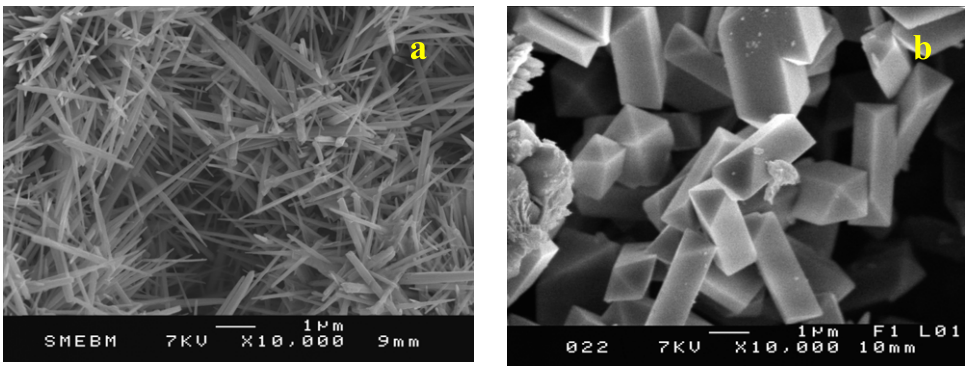

Figure 1. SEM images of needle-shaped ZnO particles with wurtzite structure (a) and double-pyramid-shaped ε-$Zn(OH)_2$ particles (b) produced by wet chemical synthesis.

dimethyl carbonate. Cell assembly was carried out under a purified argon atmosphere in a MBraun glovebox system. Electrochemical testing of the cell was performed using constant-current cycles. The current density was 10 mA g^{-1}. The cells were cycled between (0; 3.6) V.

3. Results and discussion

Two morphological forms, needle-shaped (NS) and double-pyramid-shaped (DPS), characterize the S_1, S_3 and S_2, S_4 samples, respectively. SEM investigations on ZnO powders obtained by the above procedures illustrate the NS particles in figure 1(a) and DPS particles in figure 1(b). The NS particles are thin and long hexagonal prisms, laterally faced by crystalline planes of the type $(1\bar{1}00)$ and capped with hexagonal pyramids formed by the $(10\bar{1}1)$ type crystalline planes. The DPS particles are shorter and thicker and appear as double triangular prisms bordered by crystalline planes of the type $(11\bar{2}0)$. The heads of these particles are edged by triangular roofs composed of $(11\bar{2}1)$ planes. Interestingly, using the same kind of procedure [18] reports the production of ZnO nanowire (NW) and ZnO DPS particles at synthesis temperatures >60 and 25 °C, respectively.

In this context the question immediately arises as to whether the two types of particles of different morphologies, i.e. the samples S_1, S_3 and S_2, S_4, are really particles of ZnO?

At the first sight the answer may be yes, if one takes into consideration only the absorption and luminescence spectra. ZnO as a semiconductor with a wide bandgap (3.4 eV) has been a particularly attractive candidate for research owing to its strong photoluminescence. Different ZnO nanostructured morphologies have been associated with some peculiarities in PL spectra excited with light of energy matching the fundamental absorption band. Notably, the edge absorption band has been reported at various different positions (373, 378, 380, 383, 387 and 390 nm) [22]. Two main reasons may be invoked for the variations in the position of the band-edge emission in various ZnO nanostructures: (i) one is related to the particle size—this could explain a band-edge shift towards high energy with the decrease of the dimension of the particles and (ii) another concerns the different concentration of native defects which become traps for the electrons and holes produced by the band-to-band excitation. These defects form the tail of states that in turn the band-edge transition makes less abrupt and are involved in the generation of the extra-excitonic luminescence band. In most cases, the PL of ZnO nanostructures is characterized by a weak UV edge emission related to the radiative recombination of excitons and a strong wide band located in the visible range of the optical spectrum, 500–650 nm, closely related to the surface defects. Due to the adsorption process, the PL emission strongly depends on the local surface environment. This explains, to a large extent, both the wide dispersion of reported PL data on different nanometric powders of ZnO and their dependence on the experimental measuring conditions [22, 23]. Figures 2(a) shows the PL spectra of powder samples S1 and S2. The same results were obtained on samples S_3 and S_4. For all samples, the emission spectrum at liquid nitrogen temperature (LNT) is dominated by a wide and intense emission band with the maximum around 2.00 eV that results from the radiative recombination of photo-generated carriers, holes and electrons, which have been trapped on the surface defects of particles. Figure 2(a) shows that the two types of particles, NS and DPS, display approximately the same luminescence spectrum with the difference that the wide emission band of DPS particles is up-shifted by about 0.1 eV. Additional supporting information is furnished by the excitation spectra associated with the broad emission band at about 2 eV observed at LNT for the two types of particles, figure 2(b). For the DPS particles, the experimental data reveal a shift towards higher energies although such behavior should have been observed for the NS particles for which the length/thickness ratio is smaller. The same sense of variation of the bandgap of samples S_1, S_3 and S_2, S_4 is also revealed by the absorption spectra presented in figure 2(c). Further, applying thermal annealing treatment (a few hours at 150 °C) of samples S_2 and S_4 one observes that their emission, excitation and absorption spectra coincide with those of samples S_1 and S_3. In this context, it must be concluded that samples S_1, S_3 and S_2, S_4 belong to different materials.

Raman spectroscopy, being less sensitive to surface effects, is an appropriate method to define the crystalline structure of ZnO. *A priori*, samples S_1, S_3 and S_2, S_4, by belonging to different materials, must reveal different Raman

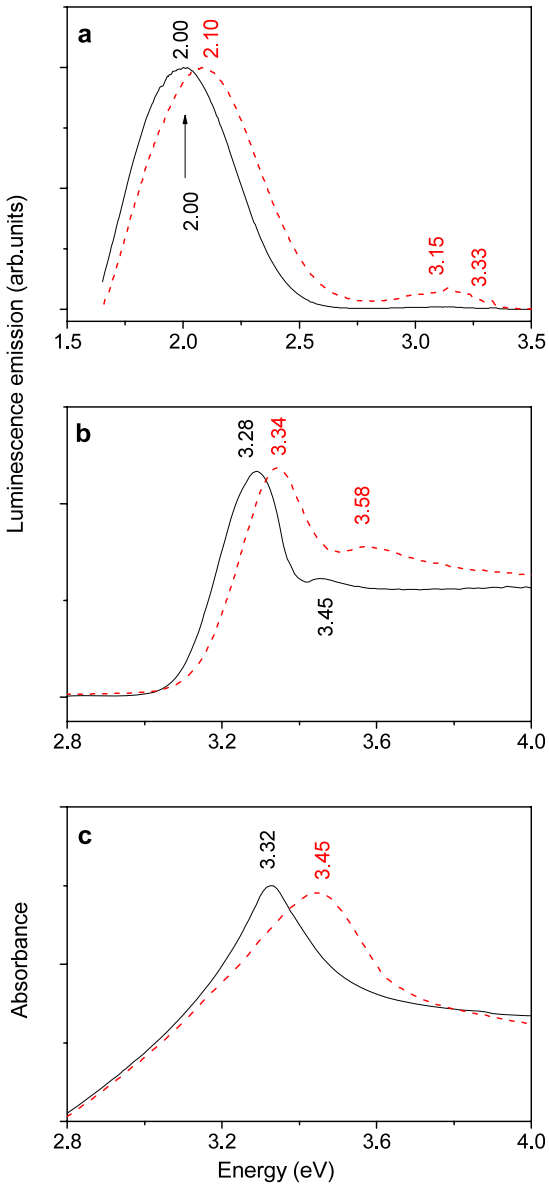

Figure 2. (a) Photoluminescence spectra at LNT under $\lambda_{exc} = 335$ nm of needle-shaped (NS) (solid line) and double-pyramid-shaped (DPS) (dashed line) particles. (b) Excitation spectra associated with the emission band at about 2 eV observed at LNT for the two types of particles: NS (solid line) and DPS (dashed line). (c) Absorption spectra of NS (solid line) and DPS (dashed line) particles.

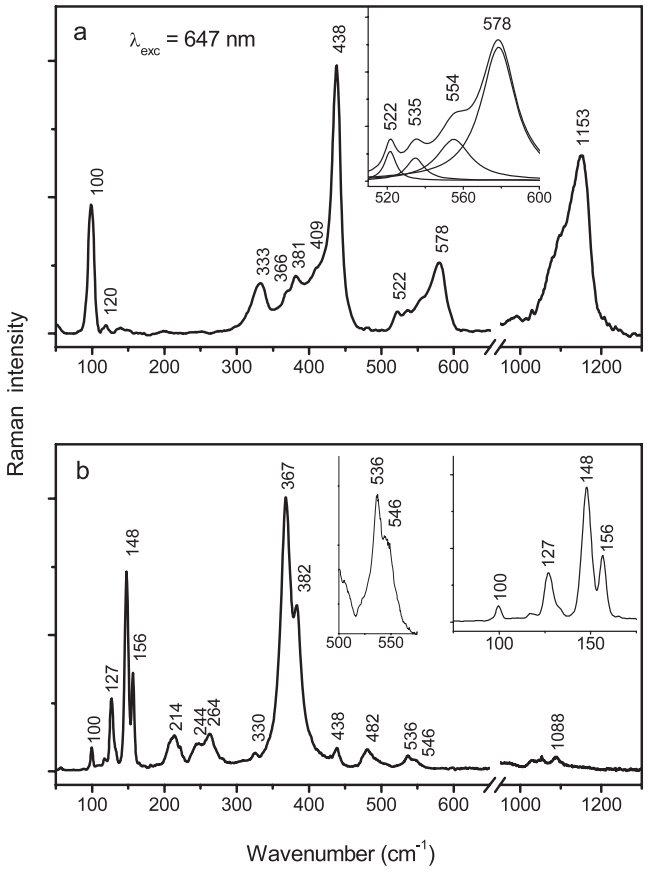

Figure 3. Raman spectra at $\lambda_{exc} = 647$ nm of needle-shaped (NS) particles (a) and double-pyramid-shaped (DPS) particles (b).

spectra. As a general observation we point out that the Raman spectra of ZnO particles of various shapes obtained by wet chemical synthesis have the signature of the WZ-like structure [1–3].

At this point, a convincing answer is provided by Raman spectroscopy—one of the most versatile methods to furnish information about material structure. Strong evidence is provided in figures 3(a) and (b) that show quite different Raman spectra for the NS and DPS particles. Figure 3(a) shows a Raman spectrum of ZnO (WZ form) already well documented in the literature [3]. For this structure, which belongs to the $C_{6v}^4(P6_3mc)$ space group in the Γ-point of the Brillouin zone, only the optical phonons are involved in first-order Raman scattering. Group theory predicts the existence of the following optical modes: $\Gamma_{opt} = A_1 + 2B_1 + E_1 + 2E_2$, where A_1 and E_1 are polar modes and are both Raman- and infrared-active, whereas the E_2 modes are non-polar and Raman-active only.

For the long-range electrostatic forces, the $A1$ and $E1$ modes split into transverse optical A_1(TO) and E_1(TO) and longitudinal optical A_1(LO) and E_1(LO) components. E_2 branches are Raman-active only and consist of two modes of low and high frequency phonons E_2(low) and E_2(high), which are associated with the vibration of the heavy Zn sublattice and oxygen atoms, respectively. B_1 modes are silent modes, infrared-and Raman-inactive. Each active vibration mode corresponds to a band in the Raman spectrum and their intensity depends on the scattering cross section of these modes. Returning to figure 3(a) one can identify the characteristic E_2 branches associated with the WZ structure of ZnO, with two components E_2(low) and E_2(high) at 99 and 438 cm^{-1}, respectively [24, 25]. In agreement with other work, in the interval 350–500 cm^{-1} three other weak bands are found, two at 409 and 380 cm^{-1} associated with E_1 (TO) and A_1(TO) modes, respectively, and the third at 333 cm^{-1} resulting from a multiple-phonon-scattering process E_2(high) − E_2(low) that occurs in the Γ-point of the Brillouin zone [24–27].

In the same figure 3(a), a wide Raman band extending from 520 to 580 cm^{-1} shows its overtone at approx. 1050–

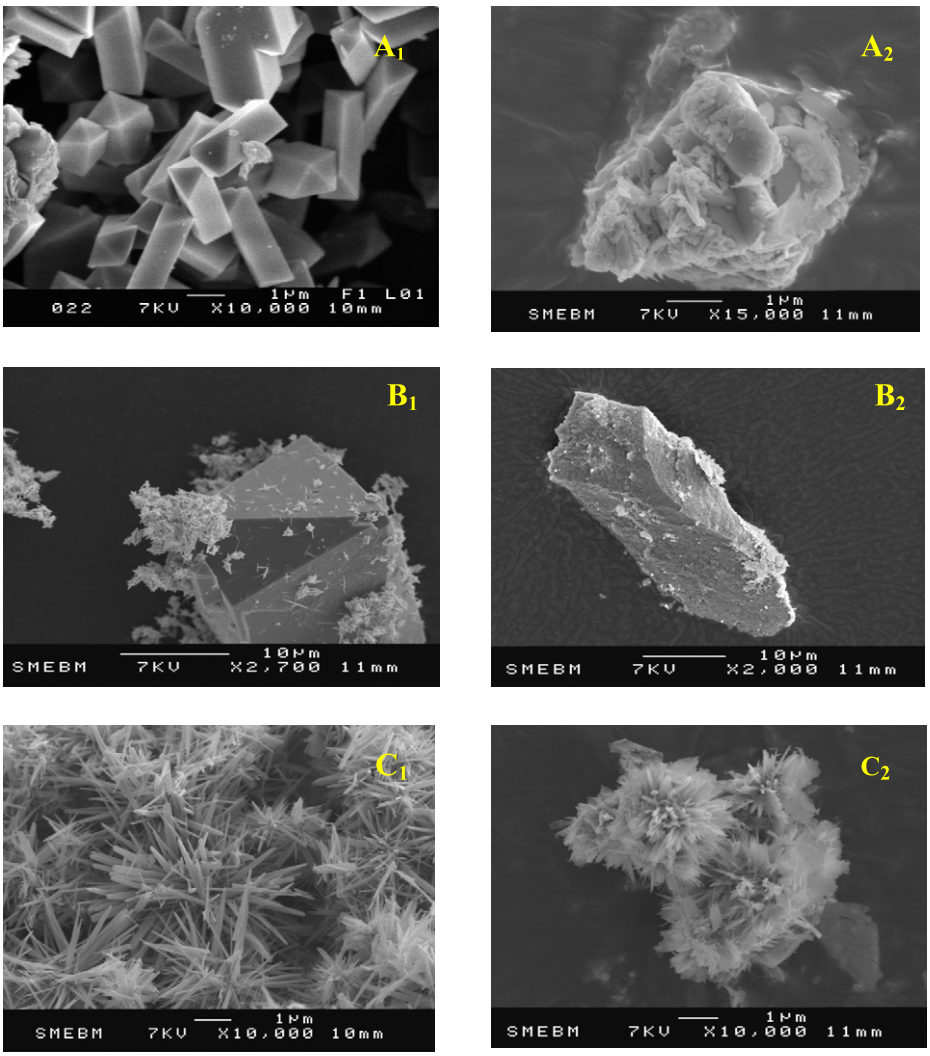

Figure 4. SEM images illustrating morphological transformation of the ZnO and ε-$Zn(OH)_2$ particles synthesized at 85 and 25 °C by thermal annealing for a few hours at 150 °C. Particles with DPS structure, synthesized at 25 °C, before and after thermal annealing are presented in figures A_1, B_1 and A_2, B_2, respectively, and the particles with NS structure synthesized at 85 °C are shown as C_1 and C_2.

1200 cm^{-1}. A detailed analysis of the former wide band discloses four components at 522, 535, 554 and 578 cm^{-1} shown in the inset of figure 4(a). The last three components may be assigned as follows: (i) similarly to the line at 333 cm^{-1} that originates in $E_2(high) - E_2$ *(low)*, the band at 535 cm^{-1} may be considered as resulting from the $E_2(high) + E_2$ *(low)* combination; (ii) the band at 554 cm^{-1} is close to 548 cm^{-1}, that is, the position predicted theoretically for the A_1 *(LO)* mode [28] and (iii) pursuant to other measurements [24, 29], the band at 578 cm^{-1} must be attributed to the E_1 *(LO)* mode.

Figure 3(b) shows that, in comparison with NS particles, the Raman spectrum of DPS particles is quite different. Inspecting the appropriate literature we have found that such a spectrum belongs to ε-$Zn(OH)_2$ [30]. ε-$Zn(OH)_2$ is known to be metastable; it transforms easily into stable ZnO in the WZ-type phase. Such a transformation can be achieved through thermal annealing for a few hours at 150 °C. The irreversible transformation is depicted in figure 4 in which the SEM images are shown before and after thermal annealing at 150 °C applied to the DPS (figures 4(A) and (B)) and NS (figure 4(C)). The morphological change is visible for most of the former particles. By thermal annealing, two main transformations are observed: (i) a disappearance of the glossy crystalline surfaces which are replaced by porous surfaces and (ii) a fragmentation of the DPS particles into smaller amorphous formations. As a result of this transformation, the newly formed structures are characterized by a WZ-type Raman spectrum. This does not occur with the NS-type particles. The thin needle structure remains unchanged and the Raman spectrum of the WZ type is preserved.

We might expect confirmation for the existence of two different materials, ZnO in the WZ phase and ε-$Zn(OH)_2$ for the NS and DPS particles, respectively, from x-ray diffraction spectra, figure 5. The strongest peak at $2\theta = 20°$ from figure 5 curve (b) corresponds to the [110] diffraction of ε-$Zn(OH)_2$. The calculated lattice parameters of the $P2_12_12_1$ space group of ε-$Zn(OH)_2$ are $a = 48\,997$ Å, $b = 51\,402$ Åand $c = 85\,121$ Å, values that are in good agreement with [31]. Thermal decomposition of ε-$Zn(OH)_2$ in a pure hexagonal ZnO phase with a wurtzite structure is well revealed by curves

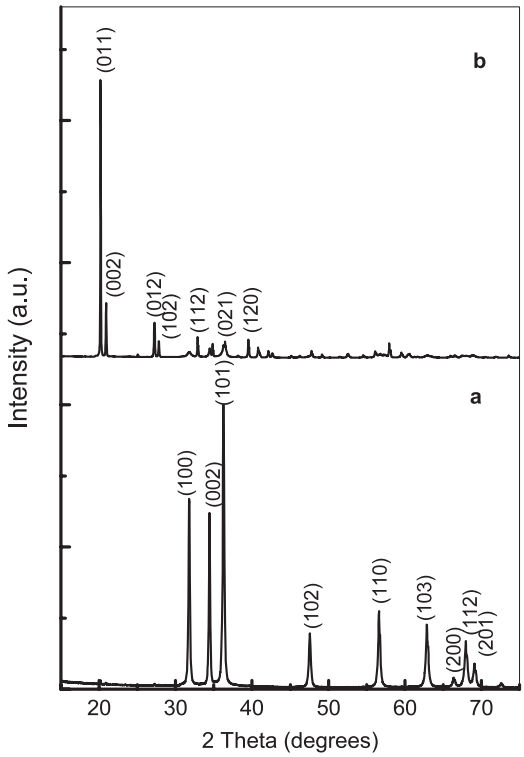

Figure 5. X-ray spectra of ZnO in wurtzite structure (curve a) and ε-$Zn(OH)_2$ (curve b).

(a) in figure 5, obtained also in the case of sample ZnO with NS.

Let us now turn to what happens when the synthesis takes place in the presence of carbon nanotubes: SWNTs, DWNTs and MWNTs. The Raman spectra of ZnO/CNs composites are shown in figure 6, where the black (solid) curves represent the Raman spectra of the carbon nanotubes (SWNTs, DWNTs, MWNTs) and the dashed curves, the Raman spectra ZnO/SWNTs, ZnO/DWNTs and ZnO/MWNTs composites obtained at 85 °C.

A short comment concerning the vibrational properties of SWNTs, DWNTs and MWNTs is necessary. In the case of SWNTs, the Raman spectrum recorded to 1064 nm shows three well-known groups of bands situated in the spectral ranges: (i) 100–350 cm^{-1}, where Raman lines at 164 and 178 cm^{-1} are associated with the radial breathing modes (RBM) of the isolated and bundled CNs, respectively [32]; (ii) 1000–1800 cm^{-1}, where two Raman bands peak at 1273 and 1594 cm^{-1}, often labeled as the D and G bands, respectively. These bands are not uniquely related to the nanotube structure; they appear in all graphitic materials. The D band, whose maximum shows dispersive behavior, is frequently associated with a disorder in the graphitic lattice or defects in nanotubes [32]. The G band, localized at 1595 cm^{-1}, is attributed to the tangential vibration mode (TM). Early studies reported that the TM band profile can be deconvoluted into four intrinsic components of Lorentzian type with the following symmetry assignments: $\omega^{-}_{E_2}$ = 1549 cm^{-1}(E_{2g}), ω^{-}_{G} = 1567 cm^{-1} ($A_{1g} + E_{1g}$), ω^{+}_{G} = 1590 ($A_{1g} + E_{1g}$) and $\omega^{+}_{E_2}$ = 1607 cm^{-1} (E_{2g}) [33]. (iii) 1800–3500 cm^{-1}, which corresponds to the second-order Raman spectrum. As a rule the most intense bands are detected at approximately twice the frequency of the D and TM band, termed 2D and 2TM, having the maxima around 2540 and 3186 cm^{-1}. Similarly with SWNTs, the Raman spectrum of DWNTs shows also three spectral ranges of interest. The first one, localized in the low frequency range, <400 cm^{-1}, contains the Raman lines associated with the RBM of the inner and outer tubes of DWNTs. Evidently, in the case of polydisperse samples, which contain DWNTs of different diameters, many pairs of lines associated with RBM will be found. The same as in the case of SWNTs, regardless of the synthesis procedure, DWNTs are obtained in the form of bundles containing many tubes [32]. Another characteristic of the DWNTs concerns the interlayer distance of the inner and outer tube that, according to the Raman calculation reported by Charlier *et al* [34], varies from 0.335 to 0.42 nm. Taking into account all this evidence, our DWNT samples in the RBM range are characterized by the following Raman line pairs which correspond to tubes with inner and outer diameter as follows: 153 cm^{-1} (1.61 nm)–266 cm^{-1} (0.88 nm), 164 cm^{-1} (1.49 nm)–316 cm^{-1} (0.74 nm) and 171 cm^{-1} (1.43 nm)–332 cm^{-1} (0.7 nm). The calculation of these diameters was carried out using the relation ω_r (cm^{-1}) = $224/d$ (nm) + 14, where ω_r corresponds to the RBM frequency and d denotes the diameter of DWNTs [32, 35] and considering that the interlayer distance is of 0.365 nm. In the spectral range 1000–1800 cm^{-1}, one finds the D and TM bands situated at 1282 and 1588 cm^{-1}, respectively, and in the interval of 2000–3500 cm^{-1} there is the second-order Raman spectrum of DWNTs which shows bands with maxima at 2545 and 3176 cm^{-1}. Both in the case of SWNTs and DWNTs, the weak D band intensity reveals nanotube samples of high-purity material. The Raman spectrum of MWNTs reveals primarily two very intense bands, D and TM, which are accompanied by a series of weak lines situated in the spectral range of RBM.

At first sight, the Raman spectra of composites ZnO/CNs presented in figures 6 appear as sum spectra of the two constituents, weighted by their different Raman scattering efficiency. In this context the question arises as to whether between constituents there is an interaction which justifies the term 'composite'? The answer is yes. We argue as follows: (i) the Raman spectra of the ZnO/CNs composites (figure 6, red (dashed) curves) show as a common feature a significant diminution in the relative intensity of the 2D Raman band that results from a breaking of bundled tubes in individual units. The high intensity of the 2D band is rather associated with the bundled state of the nanotubes. (ii) For ZnO/SWNTs the Raman spectrum discloses an up-shift of the maximum of the RBM band from 164 to 169 cm^{-1} accompanied by a decrease of its relative intensity (figure 6). Such a variation indicates a charge transfer between the two constituents; this is usually characteristic for the oxidation or the p-doping process of CNs [36]. (iii) Figure 5 shows that the G band profile narrows, and only the sharp component, located at 1594 cm^{-1}, remains. The sharpening of the G band corroborated with the decrease and up-shift of the band associated with RBM gives the signature of isolated nanotubes [37]. As expected, the

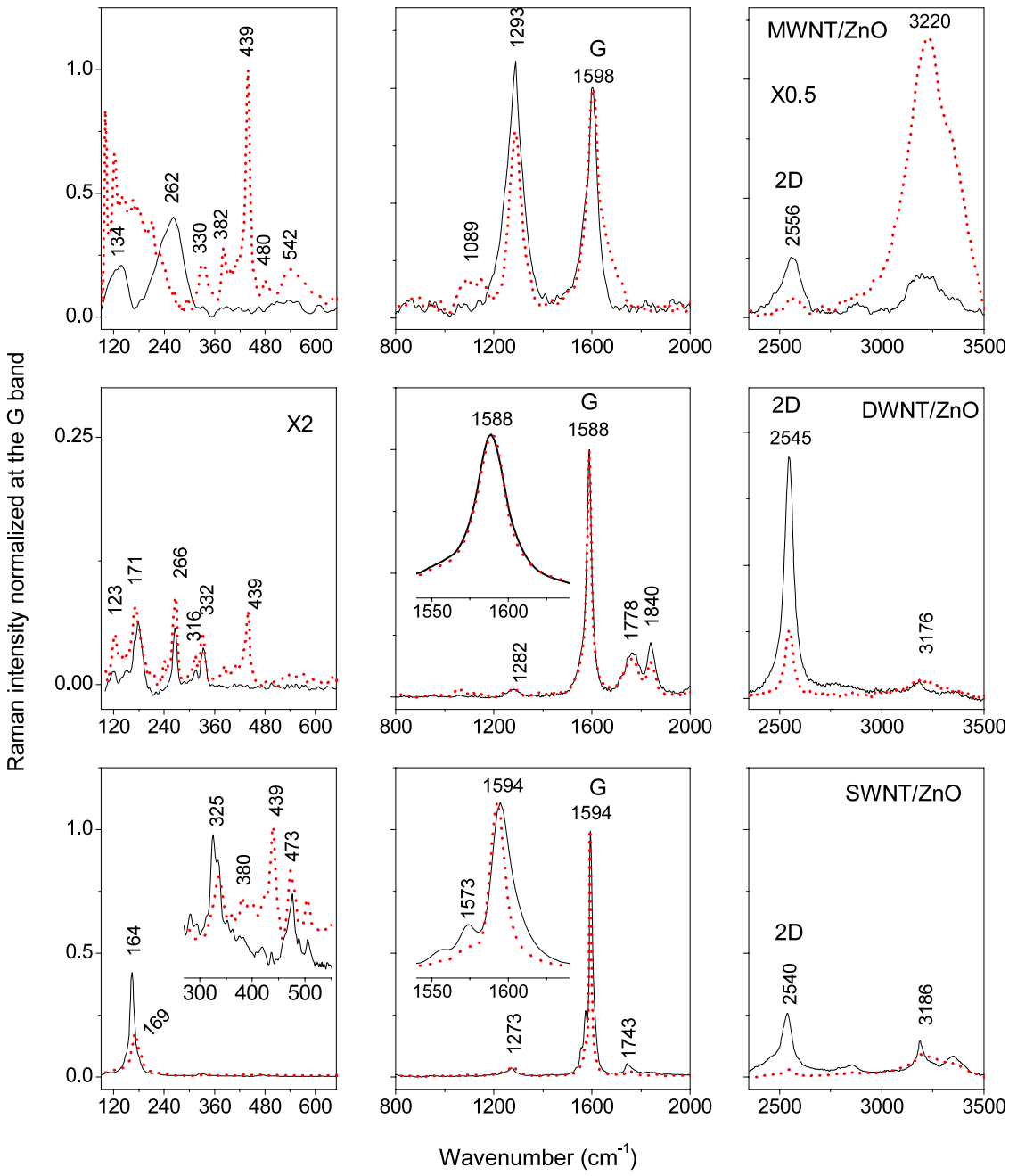

Figure 6. Red (dashed) curves: Raman spectra at $\lambda_{exc} = 1064$ nm of composites formed from needle-shaped (NS) particles and carbon nanotubes (SWNTs, DWNTs and MWNTs). Black (solid) curves: Raman spectra of carbon nanotubes.

physical attachment of various ZnO crystallites to the nanotube changes the force constants that control their motion. We may infer that this interacting process is efficient for entities of smaller size, both ZnO particles and CNs. The assumption is supported by Raman scattering experiments on DWNTs that showed neither modification of the position of the RBM band after, nor the profile of the G band.

Concerning the Raman spectra of the S_4 samples (figure 7), they appear as weighted sum of the two constituents, without any chemical interaction between them. An annealing treatment of these samples, for a few hours at 150 °C, has as a result the transformation of the ε-$Zn(OH)_2$/CNs mixture into the ZnO/CNs composite whose Raman spectra are identical with those shown in figure 6.

At this point we can conclude that the composite ZnO/CNs based on the interaction between components becomes a new material with new possibilities for practical applications. One of these may be as anode materials in rechargeable lithium ion batteries. The first study concerning the performance of ZnO as active material in lithium batteries was carried out in 2006 [38]. A probable explanation of this somewhat anomalous situation is that ZnO had been rarely used as the anode material in lithium ion batteries because of its poor cyclability compared with other transition metal

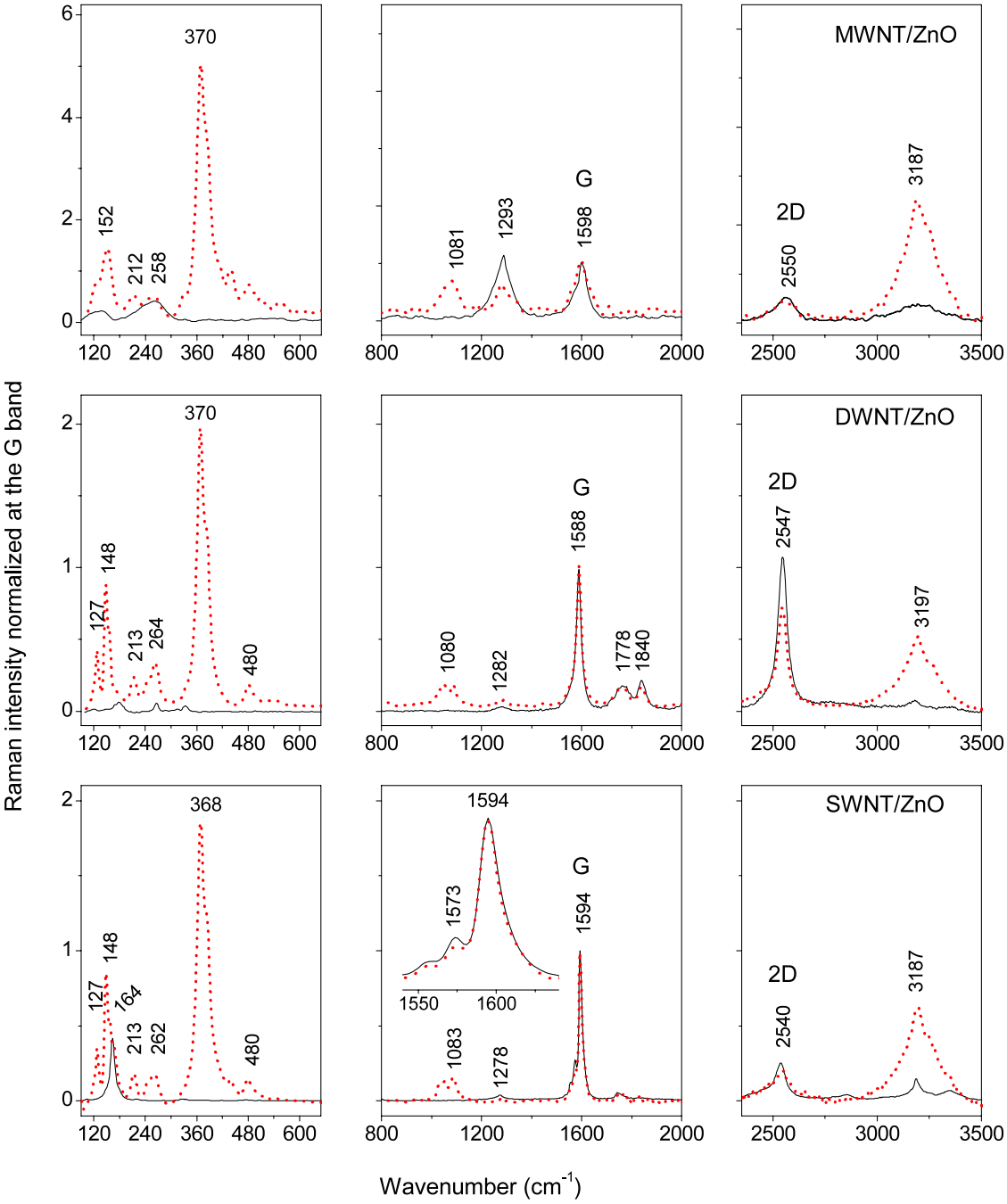

Figure 7. Red (dashed) curves: Raman spectra at $\lambda_{exc} = 1064$ nm of composites formed from double-pyramid-shaped (DPS) particles and carbon nanotubes (SWNTs, DWNTs and MWNTs). Black (solid) curves: Raman spectra of carbon nanotubes.

oxides. The main parameters responsible for the poor electrochemical performance of the ZnO electrode are low electronic conductivity and large volume change during the lithium insertion/extraction process [39, 40]. Recently, ZnO nanorod arrays have been evaluated for the negative electrode of lithium ion batteries when a capacity over 310 mA h g^{-1} after 40 cycles was reported for a rate of 0.1 mA cm^{-2} [41]. In comparison with [41] we report in this paper the capacity of the active materials of the ZnO type with WZ structure and the composite based on WZ ZnO and SWNTs at the current density of 10 mA g^{-1}. In figure 8, the initial capacity of ZnO was 980 mA h g^{-1}, that is, very close to the theoretical value (987 mA hg^{-1}). Our preliminary studies show an improvement of the specific capacity of the rechargeable lithium ion battery when the active material of the anodic electrode of needle-shaped ZnO particles (WZ structure) type is replaced with the (ZnO–NS)/CNs composite. For the two active materials a significant decrease of capacity during the first five charge–discharge cycles is observed. During the 30th charge–discharge cycle, discharge capacities of about 50 and 180 mA hg^{-1} were recorded for ZnO nanoparticles with needle-like shapes and the composite based on ZnO

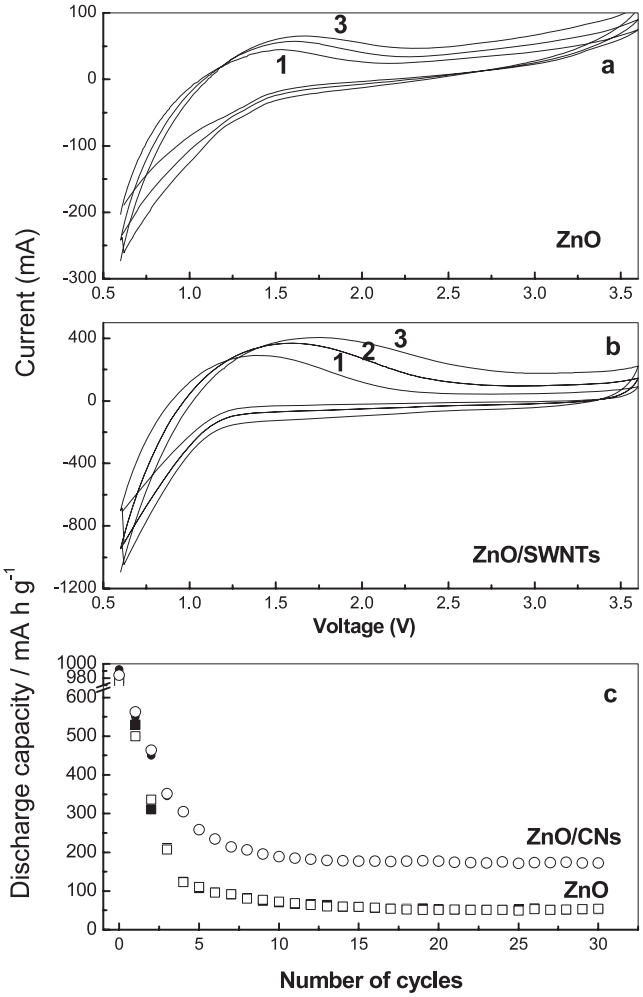

Figure 8. Cyclic voltammograms recorded with a scan rate of 10 mV s^{-1} in the presence of $LiPF_6$ + DMF + EC solution with an anode made from ZnO (a) and the ZnO/CNs composite (b). Cycle life effect on the capacity of ZnO and ZnO/CNs batteries (c).

nanoneedle/SWNTs. As for other transition metal oxides, in the case of ZnO-NS an abrupt decrease of discharge capacity that occurs during the first five charge–discharge cycles is observed [42, 43]. This behavior originates in the volume change of active particles during the lithium insertion–extraction process. If active particles do not tolerate the volume change, they pulverize into smaller particles and the electrode is strongly polarized. The high value of the discharge capacity for the active material ZnO-NS/SWNTs may be attributed to the formation of new bonds as a result of the charge transfer that occurs at the interface of the two constituents. According to [44, 45] a slowing of volume changes for the active material ZnO-NS/SWNTs is due to the presence of the carbon nanotubes. Summarizing all these, our results indicate an improvement of the electrochemical performance of the rechargeable lithium ion batteries when a ZnO nanoneedle/SWNTs composite is used as the active material. Other information concerning the electrochemical activity of the two electrodes based on ZnO nanoneedles and ZnO/SWNTs composite is provided in figures 8(a) and (b). For the cell having as an anode ZnO nanoparticles with needle-like shape, cyclic voltammograms show a broad oxidation peak at 1.54 V which is shifted to 1.61 V during the first three scans of the potential range (0.6; 3.6) V. In the case of the cell having the anode based on the ZnO/SWNTs composite, the cyclic voltammograms reveal a significant shift of the oxidation peak at 1.75 V. In addition, in this last case, larger values of current densities are observed without a change in peak shape. This fact suggests a high reversibility of the ZnO/SWNTs electrode.

4. Conclusions

We have shown that in the chemical reaction between NaOH and $ZnCl_2$ at 85 and 25 °C, respectively, particles with two different morphologies are formed: needle-shaped and double-pyramid-shaped. These particles were investigated by scanning electron microscopy, high resolution transmission electron microscopy, photoluminescence, UV–vis absorption spectroscopy, x-ray diffraction and Raman light scattering. All experimental data allow the conclusion that the needle-shaped particles correspond to ZnO with wurtzite structure while the double-pyramid-shaped particles belong to ε-$Zn(OH)_2$, which transforms by thermal annealing in ZnO. Convincing proof was supplied by Raman spectroscopy and x-ray diffraction studies. A composite of the type ZnO-NS/carbon nanotubes results when carbon nanotubes were added to the synthesis mixture. The presence of carbon nanotubes reduces the production yield of ZnO particles. For the ZnO/carbon nanotubes composites, the Raman spectra disclose a chemical interaction between components only when ZnO has a wurtzite structure. Such a material was used as the anodic electrode in a rechargeable lithium ion battery. Our preliminary studies show an improvement in the electrochemical performance of these batteries when ZnO nanoneedles/SWNTs composite is used as the active material.

Acknowledgments

This work was performed in the framework of a Scientific Co-operation between the Laboratory of Optics and Spectroscopy of the National Institute of Materials Physics, Bucharest, Romania and the Institute of Materials Jean Rouxel, Nantes, France. This research was financed by the Romanian National Authority for Scientific Research as project PN2-72-182/2008.

References

[1] Wang Z L 2004 *J. Phys.: Condens. Matter* **16** R829–58
[2] Pearton S J, Norton D P, Ip K, Heo Y W and Steiner T 2005 *Prog. Mater. Sci.* **50** 293–340
[3] Ozgur U, Alivov Y I, Liu C, Teke A, Reshchikov M A, Dogan S, Avrutin V, Cho S J and Morkoç H 2005 *J. Appl. Phys.* **98** 041301
[4] Karzel H, Potzel W, Kofferlein M, Schiessl W, Steiner M, Hiller U, Kalvius G M, Mitchell D W, Das T P, Blaha P, Schwarz K and Pasternak M P 1996 *Phys. Rev.* B **53** 11425
[5] Desgreniers S 1998 *Phys. Rev.* B **58** 14102
[6] Mujica A, Rubio A, Munoz A and Needs R J 2003 *Rev. Mod. Phys.* **75** 863
[7] Serrano J, Romero A H, Manjo F J, Lauck R, Cardona M and Rubio A 2004 *Phys. Rev.* B **69** 094306
[8] Li C, Fang G, Yuan L, Liu N, Ai L, Xiang Q, Zhao D, Pan C and Zhao X 2007 *Nanotechnology* **14** 155702

[9] Jiang L and Gao L 2005 *Mater. Chem. Phys.* **91** 313–6
[10] Ravindra S and Qzkan C S 2005 *Nanotechnology* **16** 1130
[11] Yang M, Liang T, Peng J and Chen Q 2007 *Acta Phys. Chem. Sin.* **23** 145
[12] Chen C S, Chen X H, Yi B, Liu T G, Li W H, Xu L S, Yang Z, Zhang H and Wang Y G 2006 *Acta Mater.* **54** 5401
[13] Baibarac M, Baltog I, Lefrant S, Mevellec J Y and Husanu M 2008 *Physica* E **40** 2556
[14] Liu J W, Li X J and Dai L M 2006 *Adv. Mater.* **18** 1740
[15] Zhu Y W, Elim H J, Foro Y L, Yu T, Liu Y J, Ji W, Lee J Y, Shen Z X, Wee A T S, Thong J T L and Sow C H 2006 *Adv. Mater.* **18** 587
[16] Du Y P, Hao C C and Wang G Z 2008 *Mater. Lett.* **62** 30
[17] Zhang R, Fan L, Fang Y and Yang S 2008 *J. Mater. Chem.* **18** 4964
[18] Jiang P, Zhou J J, Fang H F, Wang C Y, Wang Z L and Xie S S 2007 *Adv. Funct. Mater.* **17** 1303–10
[19] Park S S, Lee J M, Yoom S, Lee D G, Kim S J, Kim S H, Maeng S and Kim S W 2008 *Physica* E **40** 2526
[20] Wang X, Xia B, Zhu X, Chen J, Qiu S and Li J 2008 *J. Solid State Chem.* **181** 822
[21] Li P, Wei Y, Liu H and Wang X 2004 *Chem. Commun.* 2856
[22] Djurisic A B and Leung Y H 2006 *Small* **8–9** 944
[23] Baibarac M, Baltog I, Husanu M, Velula T, Bucur C, Mihut L and Preda N 2008 *J. Optoelectron. Adv. Mater.* **10** 288–93
[24] Damen T C, Porto S P S and Bell B 1966 *Phys. Rev.* **142** 570
[25] Zhang R, Yin P G, Wang N and Guo L 2009 *Solid State Sci.* **11** 865–9
[26] Calleja J M and Cardona M 1977 *Phys. Rev.* B **16** 3753
[27] Cusco R, Alarcon-Llado E, Ibanez J, Artus L, Jimenez J, Wang B and Callahan M J 2007 *Phys. Rev.* B **75** 165202
[28] Arguello C A, Rousseau D L and Porto S P S 1969 *Phys. Rev.* **181** 1351
[29] Ashkenov N, Mbenkum B N, Bundesmann C, Riede V, Lorenz M, Spemann D, Kaidashev E M, Kasic A, Schubert M, Grundmann M, Wagner G, Neumann H, Darakchieva V, Arwin H and Monemar B 2003 *J. Appl. Phys.* **93** 126
[30] Lutz H D, Jung C, Mortel R, Jacobs H and Stahl R 1998 *Spectrochim. Acta* A **54** 893
[31] Stahl R, Jung C, Lutz H D, Kockelmann W and Jacovs H 1998 *Z. Anorg. Allg. Chem.* **624** 1130
[32] Jorio A, Dresselhaus M S and Dresselhaus G 2008 *Carbon Nanotubes* (*Topics in Applied Physics* vol 111) (Heidelberg: Springer)
[33] Jorio A, Dresselhaus G, Dresselhaus M S, Souza M, Dantas M S S, Pimenta M A, Rao A M, Saito R, Liu C and Cheng H M 2000 *Phys. Rev. Lett.* **85** 2617
[34] Charlier A, McRae E, Heyd R, Charlier M F and Moretti D 1999 *Carbon* **37** 1779
[35] Rao A M, Chen J, Richter E, Schlecht U, Eklund P C, Haddon R C, Venkateswaran U D, Kwon J K and Tomanek D 2001 *Phys. Rev. Lett.* **86** 3895
[36] Stoll M, Rafailov P M, Frenzel W and Thomsen C 2003 *Chem. Phys. Lett.* **375** 625
[37] Husanu M, Baibarac M and Baltog I 2008 *Physica* E **41** 66–9
[38] Xiong H M, Wang Z D, Xie D P, Cheng L and Xia Y Y 2006 *J. Mater. Chem.* **16** 1345
[39] Belliard F, Connor P A and Irvine J T S 1990 *Ionics* **5** 450
[40] Belliard F, Connoe P A and Irvine J T S 1999 *Solid State Ion.* **123** 189
[41] Wang H, Pan Q, Chen Y, Zhao J and Yin G 2009 *Electrochim. Acta* **54** 2851
[42] Poizot P, Laruelle S, Grugeon S, Dupont L and Tarascon J M 2000 *Nature* **407** 496
[43] Taberna L, Mitra S, Poizot P, Simon P and Tarascon J M 2006 *Nat. Mater.* **5** 567
[44] Fu L J, Liu H, Zhang H P, Li C, Zhang T, Wu Y P, Holze R and Wu H Q 2006 *Electrochem. Commun.* **8** 1
[45] Zhang T, Gao J, Zhang H P, Yang L C, Wu Y P and Wu H Q 2007 *Electrochem. Commun.* **9** 886